Optical transition probabilities in Er^{3+}- and Tm^{3+}-doped $LiLa_9(SiO_4)_6O_2$ crystals

2010 J. Phys.: Condens. Matter 22 215901

(http://iopscience.iop.org/0953-8984/22/21/215901)

J. Phys.: Condens. Matter **22** (2010) 215901 (6pp) doi:10.1088/0953-8984/22/21/215901

Optical transition probabilities in Er^{3+}- and Tm^{3+}-doped $LiLa_9(SiO_4)_6O_2$ crystals

E Cantelar[1,4], M Quintanilla[1], F Cussó[1], E Cavalli[2] and M Bettinelli[3]

[1] Departamento Física de Materiales (Módulo 04), Universidad Autónoma de Madrid, E-28049 Madrid, Spain
[2] Dipartimento di Chimica Generale ed Inorganica, Chimica Analitica e Chimica Fisica, Università di Parma, I-43100 Parma, Italy
[3] Laboratorio di Chimica dello Stato Solido, DB, University of Verona and INSTM, UdR Verona, I-37134 Verona, Italy

E-mail: eugenio.cantelar@uam.es

Received 25 January 2010, in final form 6 April 2010
Published 5 May 2010
Online at stacks.iop.org/JPhysCM/22/215901

Abstract
In this work, Er^{3+} and Tm^{3+}-doped $LiLa_9(SiO_4)_6O_2$ crystals have been grown from an Li_2MoO_4 flux in the 1360–940 °C temperature range. Optical absorption spectra have been measured to obtain the experimental oscillator strengths of the transitions from the ground state to the excited levels. Judd–Ofelt calculations have been performed to estimate the Ω_2, Ω_4 and Ω_6 intensity parameters. The dynamics of selected Er^{3+} and Tm^{3+} manifolds have been investigated under selective pulsed excitation in order to determine the energy gap law by comparing the observed decay rates with the Judd–Ofelt predictions.

(Some figures in this article are in colour only in the electronic version)

1. Introduction

There is presently a renewed interest in Er^{3+} and Tm^{3+} activated materials not only because they present efficient optical transitions in the infrared spectral region but also due to their potentialities as up-conversion phosphors at the nanometric scale [1–4].

$LiLa_9(SiO_4)_6O_2$ (LLS) is a partially disordered silicate crystal belonging to the hexagonal system, with space group $P6_3/m$. The presence of specific positions for La^{3+} ions in the crystal structure should in principle be helpful to grow crystals with high RE^{3+} doping levels without involving a massive generation of extrinsic defects. Therefore, LLS crystals can be activated with trivalent rare-earth ions to yield materials with attractive luminescent properties [5–8]. Nevertheless, the basic spectroscopic properties of Er^{3+} and Tm^{3+} ions in LLS crystals have not yet been investigated and discussed.

In this work, the optical absorption spectra of Er^{3+}- and Tm^{3+}-doped crystals have been measured to obtain the experimental oscillator strengths of the transitions from the ground state to the excited levels. Judd–Ofelt calculations were performed to estimate the Ω_2, Ω_4 and Ω_6 intensity parameters and therefore the radiative lifetimes of the Er^{3+} and Tm^{3+} excited manifolds were calculated. The different experimental luminescence lifetimes have been measured and, after comparing with the Judd–Ofelt predictions, the non-radiative probabilities, W_{nr}, have been obtained. It has been found that they follow the classical dependence on the energy gap, ΔE, expressed by the 'energy gap law' formulated by Weber [9].

2. Experimental details

RE^{3+}-doped LLS crystals (RE^{3+} = Er^{3+}, Tm^{3+}) were grown from an Li_2MoO_4 flux in the 1360–940 °C temperature range [10]. In both cases the obtained crystals are well shaped, transparent and free of cracks with sizes up to 0.5 × 1 × 2 mm^3. LLS belongs to the hexagonal system, with space group $P6_3/m$ and cell parameters $a = b = 9.691$ Å and

[4] Author to whom any correspondence should be addressed.

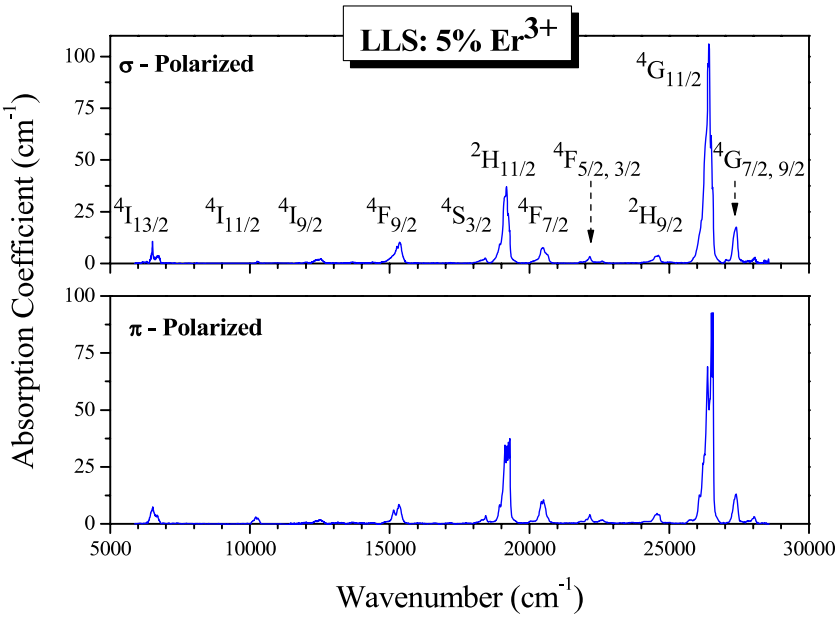

Figure 1. Polarized absorption spectra of Er^{3+}-doped $LiLa_9(SiO_4)_6O_2$.

$c = 7.162$ Å, $Z = 1$ [7]. In this crystal two La^{3+} sites are present, having different oxygen coordinations and distortions. Additionally, one of them is partially (25%) occupied by Li^+ ions with a random distribution. This implies some structural disorder and then perturbations of the crystal field around the active ions replacing La^{3+} in both sites. As a consequence, the spectral features are expected to be significantly broadened.

Absorption spectra were recorded by using a spectroscopic system made up of a halogen lamp (300 W) fitted to a 0.22 Spex Minimate monochromator as source, and a 1.26 m Spex monochromator with an RCA C31034 photomultiplier or a PbS NEP cell to detect the output radiation.

Emission spectra were obtained under CW excitation with a Ti:sapphire laser pumped with an Ar ion laser. Lifetime measurements were performed under pulsed excitation by using an optical parameter oscillator as excitation source. The geometry of luminescence collection was optimized in order to avoid radiation trapping effects. In both cases, emission spectra and lifetime measurements, the output radiation was dispersed by an ARC SpectraPro 500-i monochromator and then detected with an EMI-9558QB photomultiplier and photodiodes (InGaAs, InAs), depending on the spectral range, visible and IR, respectively.

The Raman spectrum was measured by using an Ar^+-laser operating at 488 nm as excitation source. An interferential narrow band filter was used to isolate the emitted signal from the excitation beam. The signal was focused in a fibre-coupled high resolution spectrometer (SPEX 500M) and detected by means of a CCD camera.

3. Results and discussion

3.1. Absorption spectra and Judd–Ofelt analysis

The polarized absorption spectra, at RT, of LLS: 5 mol% Er^{3+} and LLS: 6 mol% Tm^{3+} are presented in figures 1 and 2, respectively. They are composed of relatively broad bands as the result of the contribution of different optical centres. The presence of an absorption edge at wavenumbers higher than 27 000 cm^{-1} for the crystal doped with Tm^{3+} is not an artefact and is due to real absorption due to the Tm^{3+} ion. The experimental oscillator strengths, P_{exp}, of the different transitions were determined by considering the polarization of the absorption bands with a 2:1 ratio for σ:π. They were then analysed in the framework of the Judd–Ofelt (JO) theory [11, 12]. Eleven bands were considered to calculate the intensity parameters Ω_N ($N = 2, 4, 6$) of Er^{3+} and five for those of Tm^{3+}. The evaluated oscillator strengths of the transitions were fitted on the basis of the JO parametrization scheme after subtraction of the magnetic dipole contributions for the $^4I_{13/2} \leftarrow {}^4I_{15/2}$ (Er^{3+}), $^4G_{9/2} +^2 K_{15/2} + {}^2G_{7/2} \leftarrow {}^4I_{15/2}$ (Er^{3+}) and $^3H_5 \leftarrow {}^3H_6$ (Tm^{3+}) transitions. These contributions are small and not reported here.

The experimental and theoretical oscillator strength values for LLS:Er^{3+} and LLS:Tm^{3+} are summarized in tables 1 and 2, respectively. The theoretical values have been calculated by considering the reduced matrix elements given in [13] and a refractive index of $n = 1.80$ [5, 8]. The obtained intensity parameters, as well as the root-mean-square deviation of the fit (RMS), are also reported in the tables.

The spontaneous emission probabilities, branching ratios and the radiative lifetimes, τ_{rad}, for the dominant Er^{3+} and Tm^{3+} transitions in LLS are summarized in tables 3 and 4, respectively. They were estimated using the calculated intensity parameters and the reduced matrix elements published by Kaminskii [13] and correcting for the refractive index.

3.2. Non-radiative transitions: energy gap law

When energy transfer processes are negligible, the relaxation of an excited state (J) is governed by radiative and non-

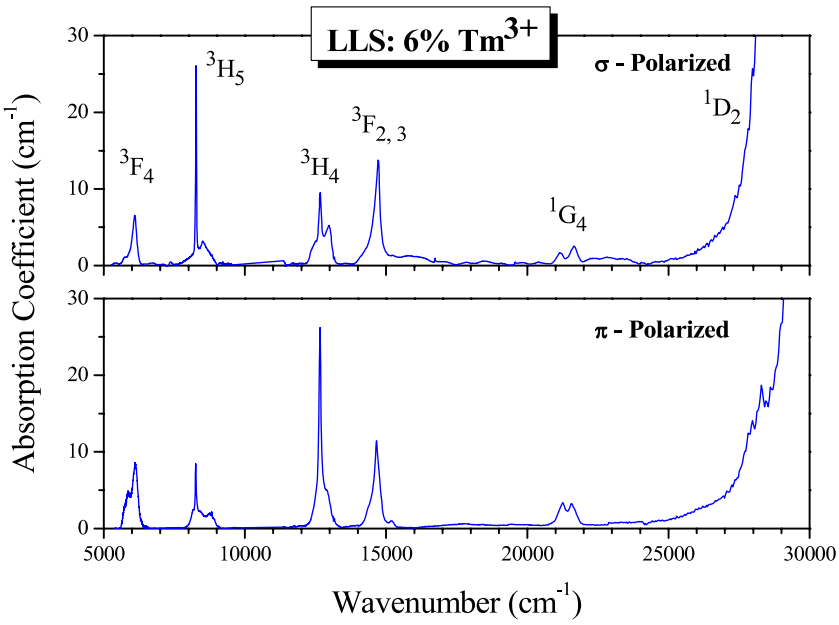

Figure 2. Polarized absorption spectra of Tm^{3+}-doped $LiLa_9(SiO_4)_6O_2$.

Table 1. Experimental and calculated oscillator strengths for Er^{3+}-doped LLS. The intensity parameters, Ω_t, the RMS and the per cent error are also indicated.

Transition	Barycentre (cm^{-1})	P_{exp} (10^{-6})	P_{th} (10^{-6})
$^4I_{15/2} \rightarrow {}^2G_{7/2,9/2}$	27 445	3.28	2.84
$^4I_{15/2} \rightarrow {}^4G_{11/2}$	26 364	18.1	16.8
$^4I_{15/2} \rightarrow {}^2H_{9/2}$	24 482	0.88	0.42
$^4I_{15/2} \rightarrow {}^4F_{5/2,3/2}$	22 238	0.56	0.40
$^4I_{15/2} \rightarrow {}^4F_{7/2}$	20 459	1.95	1.52
$^4I_{15/2} \rightarrow {}^2H_{11/2}$	19 136	8.26	9.50
$^4I_{15/2} \rightarrow {}^4S_{3/2}$	18 315	0.39	0.21
$^4I_{15/2} \rightarrow {}^4F_{9/2}$	15 243	2.56	2.72
$^4I_{15/2} \rightarrow {}^4I_{9/2}$	12 436	0.60	0.63
$^4I_{15/2} \rightarrow {}^4I_{11/2}$	10 252	0.23	0.36
$^4I_{15/2} \rightarrow {}^4I_{13/2}$	6 552	0.69	0.77
$\Omega_2 = 4.55 \times 10^{-20}$ cm^2, $\Omega_4 = 2.51 \times 10^{-20}$ cm^2, $\Omega_6 = 4.46 \times 10^{-20}$ cm^2 RMS $= 7.05 \times 10^{-7}$, RMS% $= 21$			

Table 2. Experimental and calculated oscillator strengths for Tm^{3+}-doped LLS. The intensity parameters, Ω_t, the RMS and the per cent error are also indicated.

Transition	Barycentre (cm^{-1})	P_{exp} (10^{-6})	P_{th} (10^{-6})
$^3H_6 \rightarrow {}^1G_4$	21 113	0.92	0.43
$^3H_6 \rightarrow {}^3F_{2,3}$	14 445	2.97	3.08
$^3H_6 \rightarrow {}^3H_4$	12 537	1.09	1.11
$^3H_6 \rightarrow {}^3H_5$	8 300	1.48	1.34
$^3H_6 \rightarrow {}^3F_4$	5 791	2.87	2.92
$\Omega_2 = 1.80 \times 10^{-20}$ cm^2, $\Omega_4 = 0.53 \times 10^{-20}$ cm^2, $\Omega_6 = 1.30 \times 10^{-20}$ cm^2 RMS $= 3.71 \times 10^{-7}$, RMS% $= 20$			

radiative transitions to the lower lying levels (J'). Therefore, the total relaxation probability (A_T), equal to the inverse of the experimental lifetime (τ_{exp}), can be calculated by adding both

Table 3. Calculated spontaneous emission probabilities (A), radiative branching ratios (β) and radiative lifetimes (τ_{rad}) of LLS:Er^{3+}.

Transition	A (s^{-1})	β (%)	τ_{rad} (μs)
$^2H_{11/2} \rightarrow {}^4S_{3/2}$	0.09	0.00	97
$^2H_{11/2} \rightarrow {}^4F_{9/2}$	35	0.34	
$^2H_{11/2} \rightarrow {}^4I_{9/2}$	116	1.13	
$^2H_{11/2} \rightarrow {}^4I_{11/2}$	263	2.55	
$^2H_{11/2} \rightarrow {}^4I_{13/2}$	272	2.64	
$^2H_{11/2} \rightarrow {}^4I_{15/2}$	9613	93.34	
$^4S_{3/2} \rightarrow {}^4F_{9/2}$	0.30	0.03	1110
$^4S_{3/2} \rightarrow {}^4I_{9/2}$	61	6.78	
$^4S_{3/2} \rightarrow {}^4I_{11/2}$	24	2.67	
$^4S_{3/2} \rightarrow {}^4I_{13/2}$	234	25.99	
$^4S_{3/2} \rightarrow {}^4I_{15/2}$	581	64.53	
$^4F_{9/2} \rightarrow {}^4I_{9/2}$	9	0.39	438
$^4F_{9/2} \rightarrow {}^4I_{11/2}$	54	2.36	
$^4F_{9/2} \rightarrow {}^4I_{13/2}$	113	4.95	
$^4F_{9/2} \rightarrow {}^4I_{15/2}$	2109	92.30	
$^4I_{9/2} \rightarrow {}^4I_{11/2}$	2.9	0.92	3171
$^4I_{9/2} \rightarrow {}^4I_{13/2}$	25	7.91	
$^4I_{9/2} \rightarrow {}^4I_{15/2}$	288	91.17	
$^4I_{11/2} \rightarrow {}^4I_{13/2}$	27	21.43	7906
$^4I_{11/2} \rightarrow {}^4I_{15/2}$	99	78.57	
$^4I_{13/2} \rightarrow {}^4I_{15/2}$	136	100	7359

contributions, radiative and non-radiative:

$$A_T = \frac{1}{\tau_{exp}} = \sum_{J'} A_{JJ'}(J \rightarrow J') + W_{nr}. \qquad (1)$$

Then, if the total radiative probability of a manifold is known and its experimental lifetime can be measured, the non-radiative probability could be estimated from equation (1).

On the other hand, the non-radiative relaxation probability, W_{nr}, from an excited state J to the next lower level can be

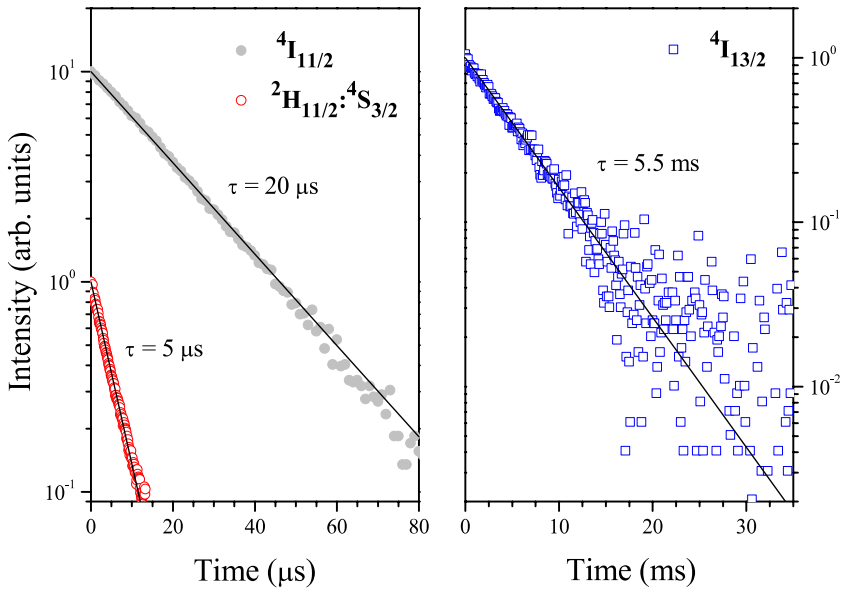

Figure 3. Temporal evolution (in a logarithmic scale) of the luminescence of $^2H_{11/2}$:$^4S_{3/2} \rightarrow {}^4I_{15/2}$, $^4I_{11/2} \rightarrow {}^4I_{15/2}$ and $^4I_{13/2} \rightarrow {}^4I_{15/2}$ Er^{3+} emission bands measured at around 550 nm, 980 nm and 1530 nm, respectively.

Table 4. Calculated spontaneous emission probabilities (A), radiative branching ratios (β) and radiative lifetimes (τ_{rad}) of LLS:Tm^{3+}.

Transition	A (s^{-1})	β (%)	τ_{rad} (μs)
$^1G_4 \rightarrow {}^3F_{2,3}$	121	6.10	504
$^1G_4 \rightarrow {}^3H_4$	256	12.90	
$^1G_4 \rightarrow {}^3H_5$	975	49.14	
$^1G_4 \rightarrow {}^3F_4$	34	1.71	
$^1G_4 \rightarrow {}^3H_6$	598	30.14	
$^3H_4 \rightarrow {}^3H_5$	66	4.17	632
$^3H_4 \rightarrow {}^3F_4$	96	6.06	
$^3H_4 \rightarrow {}^3H_6$	1421	89.77	
$^3F_4 \rightarrow {}^3H_6$	116	100	8643

described by the well-known energy gap law [14]:

$$W_{nr} = C \exp(-\alpha \Delta E) \tag{2}$$

where ΔE is the electronic energy gap, and C and α are positive constants which are characteristic of the particular host but independent of the electronic transition.

In the present work, room temperature lifetime measurements have been carried out on LLS:Er^{3+} and LLS:Tm^{3+} samples in order to determine the C and α parameters of the energy gap law, equation (2). In such kinds of measurements, crystals doped with 0.1 mol% Er^{3+} or 0.05 mol% Tm^{3+} were used to prevent possible ion–ion interactions.

In the case of LLS:Er^{3+}, the $^4I_{13/2}$, $^4I_{11/2}$ and the thermally coupled $^2H_{11/2}$:$^4S_{3/2}$ manifolds were selectively excited to study the temporal decay of their populations via the radiative transitions: $^4I_{13/2} \rightarrow {}^4I_{15/2}$ ($\lambda \approx 1530$ nm), $^4I_{11/2} \rightarrow {}^4I_{15/2}$ ($\lambda \approx 980$ nm) and $^2H_{11/2}$:$^4S_{3/2} \rightarrow {}^4I_{15/2}$ ($\lambda \approx 550$ nm). In figure 3, the temporal decays of the three emission bands are presented. As can be appreciated, the three emissions are single exponential, having a lifetime value strongly dependent on the electronic transition.

It can be pointed out that the $^2H_{11/2}$ and $^4S_{3/2}$ manifolds exhibit a common temporal decay and therefore a common lifetime value, being in thermal equilibrium. In this case, the radiative lifetime can be estimated by [15, 16]

$$\frac{1}{\tau_{rad}} = \frac{g_1 A_{rad,1} \exp(-\Delta E/kT) + g_2 A_{rad,2}}{g_1 \exp(-\Delta E/kT) + g_2} \tag{3}$$

where g_i denotes the degeneracy of the i-manifold, $A_{rad,i}$ its radiative probability, $i = 1, 2$ makes reference to the $^2H_{11/2}$ and $^4S_{3/2}$ multiplets. respectively, ΔE represents the energy gap between the two levels, k is the Boltzmann constant and T the temperature. Considering that the energy gap between the $^2H_{11/2}$ and $^4S_{3/2}$ multiplets is around $\Delta E \approx 680$ cm^{-1}, equation (3) predicts that the thermalized manifolds present a common radiative lifetime of $\tau_{rad} = 540.3$ μs at room temperature.

The dynamics of the $^3H_4$ and $^1G_4$ Tm^{3+} manifolds have also been investigated under direct pulsed excitation. In this case, the population decay was investigated by measuring the temporal evolution of the $^3H_4 \rightarrow {}^3H_6$ ($\lambda \approx 830$ nm) and $^1G_4 \rightarrow {}^3F_4$ ($\lambda \approx 650$ nm) radiative channels. Both transitions exhibit a single exponential decay, as can be seen in figure 4.

The experimental lifetimes (figures 3 and 4) are shorter than the radiative lifetimes estimated from the Judd–Ofelt calculations (tables 3 and 4). Such behaviour indicates that the multiphononic channels play an important role in the relaxation of these manifolds. Taking into account equation (1), the non-radiative transition probabilities of these Er^{3+} and Tm^{3+} levels have been evaluated. The results are depicted in figure 5 as a function of the energy gap (solid circles) between the level under consideration and the next lowest level. The least-squares fitting of the data (solid line) points out that, in LLS crystals, the non-radiative probabilities can be conveniently described by the energy gap law proposed by Weber [9], equation (2), considering that the constant parameters are

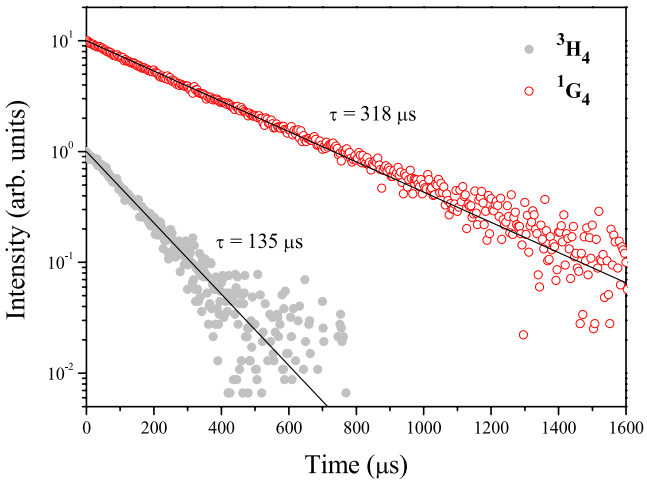

Figure 4. Temporal evolution of the luminescence associated with the $^1G_4 \rightarrow {}^3F_4$ and $^3H_4 \rightarrow {}^3H_6$ Tm^{3+} emission bands measured at around 650 nm and 830 nm, respectively.

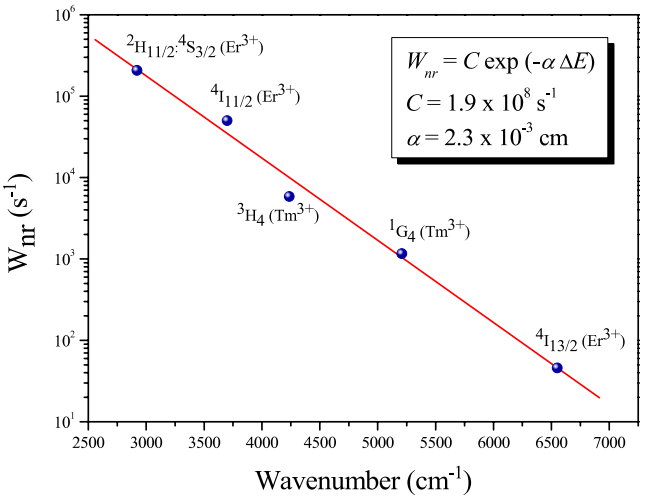

Figure 5. Non-radiative transition probabilities for different Er^{3+} and Tm^{3+} manifolds as a function of the energy gap to next lowest level (solid circles) and the least-squares fitting (solid line) to the energy gap law, equation (2).

Table 5. Comparison between the values of the C and α parameters of equation (2) for different host lattices.

	C (10^8 s^{-1})	α (10^{-3} cm^{-1})	Reference
LLS	1.9	2.3	This work
YAG	1.0	3.1	[17]
Silicate glass	14 000	4.7	[17]
YVO_4	4.0	2.6	[18]
YPO_4	4.5	1.45	[19]
$YAlO_3$	50	4.6	[20]
$LaAlO_3$	10.2	3.6	[21]

$C = 1.9 \times 10^8$ s^{-1} and $\alpha = 2.3 \times 10^{-3}$ cm. If we compare these values with those reported for other systems, see table 5, we can conclude that the efficiency of the multiphonon relaxation process is rather low in the investigated crystal.

The multiphonon relaxation rates can also be described by using the modified energy gap law proposed by van Dijk [17]:

$$W_{nr} = \beta_{el} \exp[-(\Delta E - 2\hbar\omega_{max})\alpha] \quad (4)$$

where $\hbar\omega_{max}$ is the phonon energy corresponding to the maximum vibration frequency of the host and β_{el} now becomes an electronic factor very sensitive to the host. This parameter is related to the C and α constants of equation (2) by [15]

$$\log_{10} \beta_{el} = \log_{10} C - 0.86\alpha(\hbar\omega_{max}). \quad (5)$$

In order to determine the maximum phonon energy, the non-polarized Raman spectrum was measured under 488 nm excitation. As is shown in figure 6, the energy of the maximum vibration in LLS crystals is $\hbar\omega_{max} = 943$ cm^{-1}. Assuming that this is the value of the maximum phonon energy and applying equation (5), it was found that $\log_{10}\beta_{el} = 6.41$ and therefore $\beta_{el} = 2.6 \times 10^6$. This value is in the $10^6 < \beta_{el} < 10^8$ range typical for this parameter [15, 17]. We have analysed this result in the framework of the model proposed by Marcantonatos [22], which allows estimating the expected

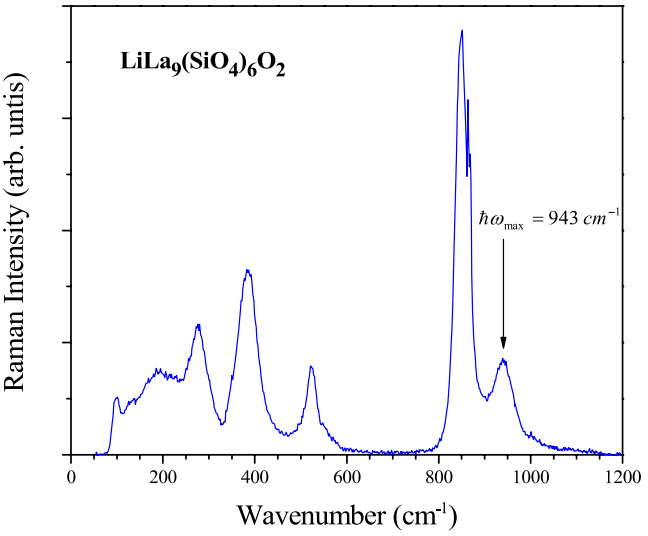

Figure 6. Non-polarized Raman spectrum measured under 488 nm excitation.

value of β_{el} by means of the following equation:

$$\beta_{el}^{calc} = \left(\frac{\pi}{2}\right)^{\frac{1}{2}} \hbar^{-1} \left[\left(\frac{\Delta E}{\hbar\omega_M}\right) - 1\right]^{-\frac{1}{2}} (\hbar\omega_M)^2 \sum_{2,4,6} \tau_\lambda ||U_\lambda||^2 \quad (6)$$

where ΔE is the gap between the emitting and the next lowest lying level, $\hbar\omega_M$ is the dominant phonon energy, τ_λ are the intensity parameters in the Judd notation and $||U_\lambda||^2$ are the squared matrix elements of the Judd–Ofelt tensor. The calculations have been carried out for the four highest phonon energies observed in the Raman spectrum and are summarized in table 6. The best agreement between experimental and calculated values is obtained for a phonon energy of 510 cm^{-1}. In the framework of the adopted model, this indicates that the latter is the main vibrational mode involved in the multiphonon

Table 6. Experimental and theoretical β_{el} values, determined for different phonon energies.

	$\hbar\omega_M$ (cm^{-1}) = 943 β_{el} (10^7)	$\hbar\omega_M$ (cm^{-1}) = 845 β_{el} (10^7)	$\hbar\omega_M$ (cm^{-1}) = 510 β_{el} (10^7)	$\hbar\omega_M$ (cm^{-1}) = 390 β_{el} (10^7)
LLS:Er^{3+}	11.3	8.5	2.30	1.16
LLS:Tm^{3+}	16.3	12.1	3.27	1.64
Average	13.8	10.3	2.79	1.40
Experimental	0.26	0.40	1.86	3.22

relaxation mechanism, the resulting value of β_{el} being 1.86×10^7. However, for the manifolds considered here, characterized by energy gaps ranging from 3000 to 6500 cm^{-1}, this would imply the creation of a large number of phonons (from 6 to 13). For this reason, we favour the attribution of the multiphonon relaxation to the highest energy phonon at 943 cm^{-1}. In this case, the agreement between the theoretical and experimental values of β_{el} is only fair (order of magnitude); as a matter of fact, this had already been noted by Marcantonatos [22].

4. Conclusions

Er^{3+}- and Tm^{3+}-doped LLS crystals, with different doping levels, have been grown by the flux growth method. The Ω_2, Ω_4 and Ω_6 intensity parameters have been estimated for both ions by means of the Judd–Ofelt theory.

The dynamics of selected excited state manifolds have been investigated upon direct excitation. The comparison between experimental lifetimes and radiative lifetimes, predicted from the Judd–Ofelt calculations, has allowed the establishment of the energy gap law in these silicate crystals. It was found that the non-radiative probabilities can be described by the classical energy gap law considering that $C = 1.9 \times 10^8$ s^{-1} and $\alpha = 2.3 \times 10^{-3}$ cm. These values are rather low in comparison with those reported for other materials, indicating that the investigated crystal is a promising host lattice for the development of new efficient emitting materials.

Additionally, the maximum phonon energy has been estimated from Raman experiments. It has been found that the maximum vibration frequency in LLS crystals takes place at 943 cm^{-1}. Alternatively, and considering this value, the non-radiative probabilities can also be described by the modified energy gap law proposed by van Dijk considering an electronic factor $\beta_{el} = 2.6 \times 10^6$.

Acknowledgments

This work was partially supported by Comunidad Autónoma de Madrid and Ministerio de Ciencia e Innovación under projects MICROSERES-CM (S2009/TIC-1476) and CRONOSOMATS (MAT2009-14102), respectively. MQ is supported by the FPU program from Ministerio de Ciencia e Innovación (AP2005-0763).

The Italian authors acknowledge the MIUR (Italian Ministry for the University and the Scientific Research) for financial support under project PRIN 2007.

References

[1] Lei Y, Song H, Yang L, Yu L, Liu Z, Pan G, Bai X and Fan L 2005 *J. Chem. Phys.* **123** 144710
[2] Suyver J F, Grimm J, van Veen M K, Biner D, Krämer K W and Güdel H U 2006 *J. Lumin.* **117** 1
[3] De G, Qin W, Zhang J, Zhang J, Wang Y, Cao C and Cui Y 2007 *J. Lumin.* **122/123** 128
[4] Nuñez N O, Míguez H, Quintanilla M, Cantelar E, Cussó F and Ocaña M 2008 *Eur. J. Inorg. Chem.* **29** 4517
[5] Steinbruegge K B, Henningsen T, Hopkins R H, Mazelsky R, Melamed N T, Riedel E P and Roland G W 1972 *Appl. Opt.* **11** 999
[6] Wang Z M, Liu Y C, Yin Y Sh and Yuan D R 2006 *Cryst. Res. Technol.* **41** 1142
[7] Bettinelli M, Speghini A, Falcomer D, Cavalli E, Calestani G, Quintanilla M, Cantelar E and Cussó F 2008 *J. Lumin.* **128** 738
[8] Cavalli E, Calestani G, Belletti A, Bettinelli M and Speghini A 2009 *Opt. Mater.* **31** 1340
[9] Weber M J 1968 *Phys. Rev.* **171** 283
[10] Setoguchi M 1990 *J. Cryst. Growth* **99** 879
[11] Judd B R 1962 *Phys. Rev.* **127** 750
[12] Ofelt G S 1962 *J. Chem. Phys.* **37** 511
[13] Kaminskii A A 1996 *Crystalline Lasers: Physical Processes and Operating Schemes* (Boca Raton, FL: CRC Press)
[14] Riseberg L A and Moos H W 1968 *Phys. Rev.* **174** 429
[15] Reisfeld R 1987 *Spectroscopy of Solid-State Laser Type Materials* (New York: Plenum) p 343
[16] Muñoz J A, Di Paolo R E, Duchowicz R, Tocho J O and Cussó F 1998 *Solid State Commun.* **107** 487
[17] van Dijk J M F and Schuurmans M F H 1983 *J. Chem. Phys.* **78** 5317
[18] Ermeneux F S, Goutaudier C, Moncorgé R, Sun Y, Cone R L, Zannoni E, Cavalli E and Bettinelli M 2000 *Phys. Rev.* B **61** 3915
[19] Zheng H and Meltzer R S 2007 *J. Lumin.* **22/23** 478
[20] Weber M J 1973 *Phys. Rev.* B **8** 54
[21] Deren P, Mahiou R and Goldner P 2009 *Opt. Mater.* **31** 465
[22] Marcantonatos M D 1986 *J. Chem. Soc. Faraday Trans.* **82** 609